Entanglement between an Electron and a Nuclear Spin $\frac{1}{2}$

M. Mehring, J. Mende, and W. Scherer

2. Physikalisches Institut, Universität Stuttgart, Pfaffenwaldring 57, 70550 Stuttgart, Germany

(Received 29 August 2002; published 15 April 2003)

We report on the preparation and detection of entangled states between an electron spin 1/2 and a nuclear spin 1/2 in a molecular single crystal. These were created by applying pulses at ESR (9.5 GHz) and NMR (21 MHz, 46 MHz) frequencies. Entanglement was detected by using a special entanglement detector sequence based on a unitary back transformation including phase rotation.

DOI: 10.1103/PhysRevLett.90.153001 PACS numbers: 33.35.+r, 03.65.Ud, 03.67.–a, 76.30.–v

The entanglement between two spins 1/2 is at the heart of quantum mechanics. Ever since a so-called "paradox" was formulated by Einstein, Podolsky, and Rosen (EPR) [1], referring to local measurements performed on the individual spins of a delocalized entangled pair, properties of entanglement and its consequences for quantum physics has been discussed in great detail [2]. In the context of quantum information processing entanglement has been considered as a resource for quantum parallelism (speedup of quantum computing) [3–5] and quantum cryptography [6,7]. A number of these quantum algorithms have been demonstrated by NMR (nuclear magnetic resonance) quantum computing [8–10].

In this contribution we report on the experimental preparation and observation of the entangled states of an electron spin $S = 1/2$ and a nuclear spin $I = 1/2$ in a crystalline solid. Besides its principal aspects these states might become important elements in a solid state spin quantum computer. The spins considered here are a proton and a radical (unpaired electron spin) produced by x-ray irradiation of a malonic acid single crystal [11]. This leads to the partial conversion of the CH_2 group of the malonic acid molecule to the radical $^{\bullet}CH$ where the dot marks the electron spin. In a strong magnetic field the following four Zeeman product states $|m_S m_I\rangle = |\uparrow\uparrow\rangle, |\uparrow\downarrow\rangle, |\downarrow\uparrow\rangle, |\downarrow\downarrow\rangle$ exist where the arrows label the $\pm 1/2$ states of the electron and the nuclear spin. Equivalently we use a qubit labeling as $|m_S m_I\rangle = |00\rangle, |01\rangle, |10\rangle, |11\rangle$ or alternatively a state labeling $|j\rangle = |1\rangle, |2\rangle, |3\rangle, |4\rangle$. The energy level diagram corresponding to the electron-proton spin system is shown in Fig. 1, where we have also indicated the possible ESR ($\Delta m_S = \pm 1$) and NMR transitions ($\Delta m_I = \pm 1$) of the individual spins by solid arrows. Unitary transformation is applied to the spin system by selective pulses with rotation angle β of the type $P_{S,I}^{jk}(\beta)$, where $j \neq k \in \{1, 2, 3, 4\}$ labels the transition and the subscript S, I is added for convenience to distinguish between ESR and NMR transitions. Pulses for spins 1/2 in the x or y direction of the rotating frame are unitary transformations and can be expressed in terms of Pauli matrices as

$$P_{S,I}^{jk}(\beta) = I_4 \cos(\beta/2) - i\sigma_{x,y} \sin(\beta/2), \qquad (1)$$

where I_4 is the 4×4 identity matrix. Note that a $\pi/2$ pulse in the y direction (y pulse) performs a similar transformation as the Hadamard transform and is used here as a pseudo Hadamard transform. What we are aiming at are states of the type

$$\Psi^{\pm} = \frac{1}{\sqrt{2}}(|\uparrow\downarrow\rangle \pm |\downarrow\uparrow\rangle) \quad \text{and} \quad \Phi^{\pm} = \frac{1}{\sqrt{2}}(|\uparrow\uparrow\rangle \pm |\downarrow\downarrow\rangle). \qquad (2)$$

These represent all four possible entangled states of a two qubit system, also called the Bell states of two spins 1/2. They correspond to a superposition of the states in Fig. 1 connected by dashed arrows.

Starting from the pure state $|\downarrow\uparrow\rangle$ a selective NMR pulse $[P_I^{34}(\pi/2)]$ followed by a selective ESR pulse $[P_S^{24}(\pi)]$ suffice to create Ψ^- (except for an overall minus sign):

$$|\downarrow\uparrow\rangle \xrightarrow{P_I^{34}(\pi/2)} \frac{1}{\sqrt{2}}(|\downarrow\uparrow\rangle + |\downarrow\downarrow\rangle) \xrightarrow{P_S^{24}(\pi)} -\frac{1}{\sqrt{2}}(|\uparrow\downarrow\rangle - |\downarrow\uparrow\rangle). \qquad (3)$$

All other Bell states can be created in a similar way by varying the excitation transition. Electron spin resonance (ESR) was performed at the X band (9.39 GHz) at $T = 30$ K. The two well resolved ESR lines due to the $^{\bullet}CH$

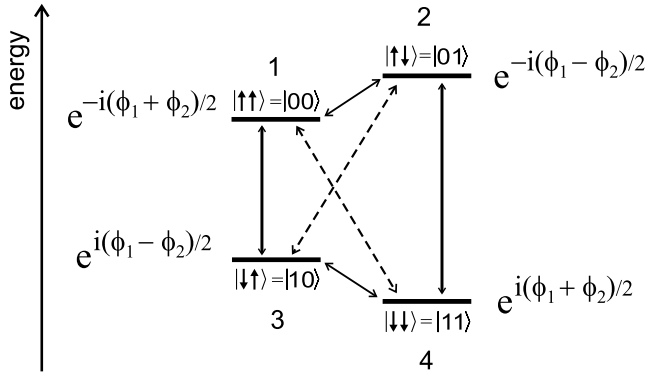

FIG. 1. Schematic diagram of the four energy levels of a two spin system with $S = 1/2$ and $I = 1/2$. The solid arrows denote allowed transitions. The dashed arrows indicate forbidden transitions, corresponding to entangled states. The phase dependence of the quantum states under z rotations is also indicated (see text).

proton depend on the orientation of the single crystal and were observed at magnetic fields of 331.99 and 334.54 mT with a linewidth of 0.47 mT for the ESR and about 1 MHz for the ENDOR (electron-nuclear double resonance) line. There are two different proton NMR transitions. We applied pulsed ENDOR techniques to both of them at the frequencies of 21.39 MHz ($1 \leftrightarrow 2$ transition) and 45.56 MHz ($3 \leftrightarrow 4$ transition). Since we are dealing with an ensemble of spins we invoke the density matrix description in the following.

In the high temperature approximation we express the Boltzmann spin density matrix as $\rho_B = (1 - K_B)\frac{1}{4}I_4 + K_B \cdot \rho_P$ with $K_B = \mu_B B_0/3k_B T$ (for $g = 2$) with $\rho_P = \frac{1}{4}I_4 - \frac{3}{2}S_z$. Since the Larmor frequency of the nuclear spins is much smaller than the one of the electron spins we ignore here any polarization of the nuclear spins. In order to prepare for a pseudopure density matrix we start from a truncated Boltzmann density matrix of the form $\rho'_P = -\frac{3}{2}S_z$ which leads to equal population of the states $(|10\rangle; |1\bar{1}\rangle)$ and $(|01\rangle; |00\rangle)$.

We have prepared the pseudopure diagonal density matrix ρ_{10} with diagonal components $\{0, 0, 1, 0\}$ by performing the pulse sequence $P_S^{24}(109.47°)$ followed by, after a waiting time of several microseconds to let the transverse components decay, a $P_S^{12}(\pi/2)$ pulse to equalize the 1 and 2 populations. After a waiting time of 20 μs all transients have decayed and we obtained the pseudopure density matrix as is shown in Eq. (4):

$$\rho_{10} = \begin{pmatrix} 0.01 & 0 & 0 & 0 \\ 0 & -0.06 & 0 & 0 \\ 0 & 0 & 1.02 & 0 \\ 0 & 0 & 0 & 0.03 \end{pmatrix}. \qquad (4)$$

Density matrix tomography has been applied in liquid state NMR quantum computing (for a recent example, see [12,13]) to provide quantitative measures of the quantum states. We have adopted these methods for the special case of electron-nuclear quantum states as discussed here. The tomography of the pseudopure density matrix requires one to determine only diagonal terms. Population differences were determined by irradiating selectively the corresponding transitions and measuring the amplitudes of the Rabi precession frequency. After setting the sum of the resulting elements of the truncated diagonal density matrix to zero and adding a quarter of the 4×4 identity matrix the final density matrix as quoted in Eq. (4) was obtained. We have used this density matrix as the initial density matrix for creating the pseudoentangled states $\Psi^{\pm}$ and $\Phi^{\pm}$.

As an example we treat the Ψ^- state in detail. The preparation of Ψ^- proceeds by applying selective ESR and NMR pulses, which transforms ρ_{10} into ρ_{Ψ^-} as was outlined in Eq. (3). Alternatively the creation of the Ψ^+ state can be achieved by the y-pulse sequence $P_I^{34}(-\pi/2)$ followed immediately by $P_S^{24}(\pi)$. In order to prepare all four Bell states $\Psi^{\pm}$ and $\Phi^{\pm}$ we need to apply selective excitations to three connected states. We have restricted ourselves here to the sublevels (2, 3, 4) for creating the $\Psi^{\pm}$ states and to (1, 3, 4) for creating the $\Phi^{\pm}$ states. Creating the $\Phi^{\pm}$ states can be achieved by the selective y-pulse sequence $P_I^{34}(\pi/2)$ followed immediately by $P_S^{13}(\pm\pi)$ applied to the initial density matrix ρ_{11}. We have prepared this pseudopure density matrix in a similar way as was discussed in the case of ρ_{10}. In all these experiments we have used the following typical values: 32 ns for the ESR π pulses and 1.2 μs for the NMR $\pi/2$ pulses. Entanglement is achieved with these in about 1.2 μs.

In order to prove that the Ψ^- state has indeed been created we apply a density matrix tomography which is based on the phase dependence of the entangled state as already sketched in Fig. 1. By utilizing this phase dependence one could avoid the collapse of the wave function even for a pure state. The phase factors noted there represent the phase dependence of the corresponding states under rotation about the quantization axis (z axis). This corresponds to the unitary transformations $U_{S_z} = \exp(-i\phi_1 S_z)$ and $U_{I_z} = \exp(-i\phi_2 I_z)$ leading to $U_{S_z}U_{I_z}|m_S m_I\rangle = \exp[-i(\phi_1 m_S + \phi_2 m_I)]|m_S m_I\rangle$. A single ESR transition ($\Delta m_S = \pm 1$) will have a phase dependence ϕ_1 under z-axis rotation, whereas a single NMR transition ($\Delta m_I = \pm 1$) will have a phase dependence ϕ_2. Each of the entangled states $\Psi^{\pm}$ and $\Phi^{\pm}$ is characterized by a linear combination $\phi_1 \pm \phi_2$ of both phases. This is another manifestation of the fact that these states are global states and no local measurement on the single qubits reveals any information about the entangled state.

Since the entangled state is not directly observable we need to transform it to an observable state. Our entangled state detector therefore corresponds to a unitary back transformation comprised of, e.g., $P_S^{24}(\pi)$ followed by $P_I^{34}(\pi/2)$ applied to the state Ψ^-. In order to distinguish entangled states from other superposition states we encode their character in the phase dependence under z rotation as discussed before. Therefore we apply phase shifted x pulses of the type $P_S^{24}(\pi, \phi_1)$ and $P_I^{34}(\pi/2, \phi_2)$ which corresponds to a rotation about the z axis by the angles ϕ_1 and ϕ_2. The complete $\Psi^{\pm}$ detector sequence now reads

$$U_d^{\Psi}(\phi_1, \phi_2) = P_I^{34}(\pi/2, \phi_2)P_S^{24}(\pi, \phi_1). \qquad (5)$$

Since our observable is the ESR transition intensity, detected via an electron spin echo, the entangled state tomography corresponds to the evaluation of the following signal strength for $\Psi^{\pm}$:

$$S_d^{\Psi}(\phi_1, \phi_2) = \mathrm{tr}\{2S_z^{24}U_d^{\Psi}|\Psi^{\pm}\rangle\langle\Psi^{\pm}|U_d^{\Psi\dagger}\}, \qquad (6)$$

where S_z^{24} is the fictitious spin 1/2 of the $2 \leftrightarrow 4$ transition. With the current definitions we obtain the expression

$$S_{\mathrm{d}}^{\Psi}(\phi_1, \phi_2) = -\tfrac{1}{2}[1 \pm \cos(\phi_1 - \phi_2)]. \quad (7)$$

Alternatively we have used for the detection of the $\Phi^{\pm}$ states the sequence

$$U_{\mathrm{d}}^{\Phi}(\phi_1, \phi_2) = P_I^{34}(\pi/2, \phi_2) P_S^{13}(\pi, \phi_1), \quad (8)$$

leading to a detector signal for $\Phi^{\pm}$,

$$S_{\mathrm{d}}^{\Phi}(\phi_1, \phi_2) = \mathrm{tr}\{2S_z^{13} U_{\mathrm{d}}^{\Phi} |\Phi^{\pm}\rangle\langle\Phi^{\pm}| U_{\mathrm{d}}^{\Phi\dagger}\} \quad (9)$$

with

$$S_{\mathrm{d}}^{\Phi}(\phi_1, \phi_2) = -\tfrac{1}{2}[1 \pm \cos(\phi_1 + \phi_2)]. \quad (10)$$

The phase shifts were implemented by incrementing the phase of the individual detection pulses in consecutive experiments according to $\phi_j(n) = \Delta\omega_j n \Delta t$ with $j = 1, 2$. The artificial phase frequencies $\Delta\omega_j = 2\pi\Delta\nu_j$ were arbitrarily chosen as $\nu_1 = 2.0$ MHz and $\nu_2 = 1.5$ MHz. Examples of different phase increments are shown in Fig. 2.

The corresponding spectra (see Fig. 3) are obtained after Fourier transformation of the phase interferograms. The phase frequency of the entangled states clearly shows the expected peaks at the frequency $\nu_1 - \nu_2 = 0.5$ MHz for the Ψ^- state [see Eq. (7)] and at frequency $\nu_1 + \nu_2 = 3.5$ MHz for the Φ^+ state [see Eq. (10)].

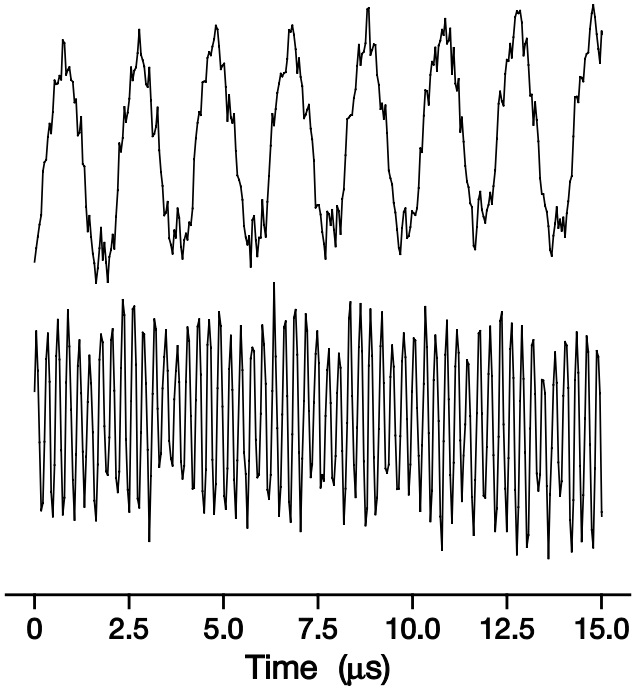

FIG. 2. Phase interferograms versus time $n\Delta t$ for Ψ^- (top) and Φ^+ (bottom). Note that the phase interferogram for Ψ^- leads to an "oscillation" with the phase difference $\phi_1 - \phi_2$ [see Eq. (7)], whereas the state Φ^+ exhibits a phase oscillation with $\phi_1 + \phi_2$ [see Eq. (10)].

The artifacts seen in Fig. 3 are residual contributions of the single transition phase frequencies $\nu_1 = 2.0$ MHz and $\nu_2 = 1.5$ MHz. Another artifact at 4 MHz is of electronic origin from the synthesis of the phase shifted microwave pulses. It should be noted that the phase interferograms and the corresponding spectra were obtained after *purification* of the pseudoentangled state. The creation of these states is complicated by the large inhomogeneous linewidth of the transitions. The corresponding selective excitation must be described by a distribution of rotation angles. However, a precise setting of these angles is required for creating the entangled states. The off-angle settings create a *contamination* with single transition coherences which show up as ν_1 and ν_2 phase frequencies. These unwanted frequencies can be eliminated by utilizing their antisymmetry under a π phase shift because the entangled state phase coherences are invariant under a combined phase shift of both ESR and NMR coherences by π. The entangled states were prepared by adding the signals with and without a combined π phase shift. This is in line with the *temporal averaging* procedure also applied in NMR quantum computing. More details will be published elsewhere.

In order to quantify the degree of pseudoentanglement we have performed a density matrix tomography as follows. The tomography of the diagonal part of the density matrix was performed as discussed already for the pseudopure states. The off-diagonal parts for the entangled states could be obtained from the phase interferograms by

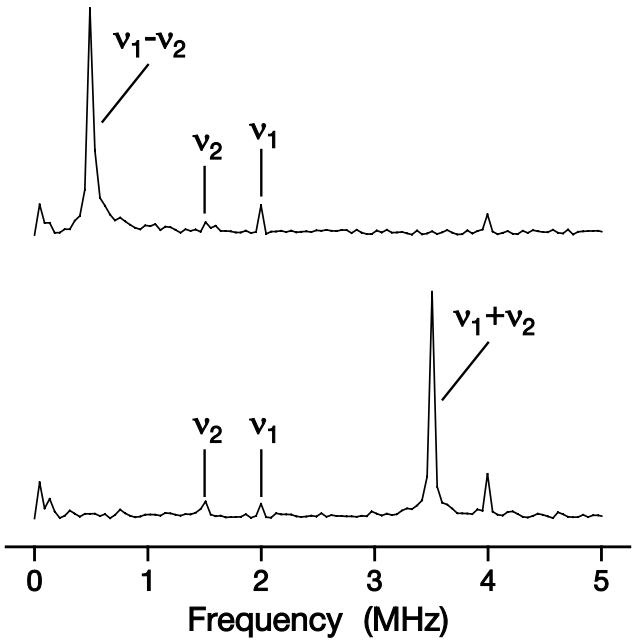

FIG. 3. Fourier transform of the phase interferograms shown in Fig. 2 for phase frequencies $\nu_1 = 2.0$ MHz and $\nu_2 = 1.5$ MHz (see text). Top (Ψ^-): $\nu_1 - \nu_2 = 0.5$ MHz; bottom (Φ^+): $\nu_1 + \nu_2 = 3.5$ MHz. For the artifacts, see text.

measuring the amplitudes of the $\phi_1 \pm \phi_2$ signals. In order to quantify these and other off-diagonal values we have applied combined Rabi precession investigations of the different ESR and NMR coherences. As a result we could obtain most of the off-diagonal matrix elements. Others were zero by the fact that the transition frequencies were widely separated from the excitations and no coherences could have been excited there. We also assumed that the density matrix of the entangled state is symmetric. Moreover, there is some loss of signal during the tomography sequence. We therefore scaled all off-diagonal elements in such a way that the condition $\mathrm{tr}\{\rho_{\mathrm{ent}}^2\} = 1$ is fulfilled. As a final result we obtained for the EPR state

$$\rho_{\Psi^-}^{\mathrm{exp}} = \begin{pmatrix} -0.02 & 0.00 & 0.0 & 0.00 \\ 0.00 & 0.55 & -0.47 & 0.06 \\ 0.0 & -0.47 & 0.50 & 0.02 \\ 0.00 & 0.06 & 0.02 & -0.03 \end{pmatrix}, \qquad (11)$$

where one expects the values 0.5 on the diagonal and -0.5 at the off-diagonal sites. The experimental values lead to a surprisingly large fidelity of

$$F_{\Psi^-} = \mathrm{tr}\{\rho_{\Psi^-}^{\mathrm{exp}} \rho_{\Psi^-}\}/\mathrm{tr}\{\rho_{\Psi^-}^2\} = 0.99. \qquad (12)$$

This should, however, not be overinterpreted since it includes the mentioned purification procedure and the assumption that decoherence losses during the tomography sequence can be accounted for by scaling the off-diagonal elements to obtain $\mathrm{tr}\{\rho_{\Psi^-}^2\} = 1$. Similar results were obtained for ρ_{Ψ^+} and $\rho_{\Phi^\pm}$ which will be published elsewhere.

Our goal was not so much to achieve a high degree of entanglement, but to demonstrate, as we believe for the first time, how entanglement of nuclear and electron spins can be achieved in a solid material. With special materials at hand, where the intrinsic linewidth is appreciably narrower than in our case, a high degree of entanglement is achievable and detectable with the algorithms applied in this Letter.

A brief note on the entanglement of mixed state might be appropriate. We have used here an ensemble of electron-nuclear spin pairs described by a mixed state density matrix. As in all so far published NMR quantum computing experiments the corresponding entangled states would be better termed *pseudoentangled states* [8–10]. Space does not allow us to enter into a detailed discussion on how to proceed from *pseudoentanglement* to real entanglement. However, we point out that the same pulse sequences used here could be applied to a pure state electron-nuclear spin pair in order to create the discussed entangled states. Also the same Bell state detection sequences as proposed here would apply. In fact, the same phase dependence would be observed for pure states. Moreover, the experiments presented here would reach the quantum limit (see Warren *et al.* [14]) according to the positive partial transpose criterion [15,16] at $\tanh(\hbar\omega_S/2k_BT) = \sqrt{2}$ which corresponds to a temperature $T_Q = 2.576$ K for an ESR frequency of 95 GHz, well in reach with current technology.

Details of the density matrix tomography, the purification procedure, and the results for the complete set of Bell states will be presented in a forthcoming publication.

We acknowledge financial support by the German Bundesministerium für Bildung und Forschung (BMBF).

[1] A. Einstein, B. Podolski, and N. Rosen, Phys. Rev. **41**, 777 (1935).
[2] D. M. Greenberger, M. A. Horne, and A. Zeilinger, in *Bell's Theorem, Quantum Theory and Conceptions of the Universe* (Kluwer Academic Publishers, Dordrecht, 1989), p. 69.
[3] D. Deutsch, Proc. R. Soc. London A **400**, 97 (1985).
[4] D. Deutsch and R. Josza, Proc. R. Soc. London A **439**, 553 (1992).
[5] L. K. Grover, Phys. Rev. Lett. **79**, 325 (1997).
[6] C. H. Bennet and G. Brassard, in *Proceedings of the IEEE International Conference on Computers, Systems and Signal Processing* (IEEE, New York, 1984).
[7] C. H. Bennet, F. Besette, G. Brassard, L. Salvail, and J. Smolin, J. Cryptology **5**, 3 (1992).
[8] D. G. Cory, A. F. Fahmy, and T. F. Havel, Proc. Natl. Acad. Sci. U.S.A. **94**, 1634 (1997).
[9] N. A. Gershenfeld and I. L. Chuang, Science **275**, 350 (1997).
[10] E. Knill, I. Chuang, and R. Laflamme, Phys. Rev. A **57**, 3348 (1998).
[11] H. M. McConnell, C. Heller, T. Cole, and R. W. Fessenden, J. Am. Chem. Soc. **82**, 766 (1960).
[12] G. Teklemariam, E. M. Fortunato, M. A. Pravia, T. F. Havel, and D. G. Cory, Phys. Rev. Lett. **86**, 5845 (2001).
[13] G. Teklemariam, E. M. Fortunato, M. A. Pravia, Y. Sharf, T. F. Havel, D. G. Cory, A. Bhattaharyya, and J. Hou, Phys. Rev. A **66**, 012309 (2002).
[14] W. S. Warren, N. Gershenfeld, and I. Chuang, Science **277**, 1688 (1997).
[15] A. Peres, Phys. Rev. Lett. **77**, 1413 (1996).
[16] M. Horodecki, P. Horodecki, and R. Horodecki, Phys. Lett. A **223**, 1 (1996).